ACS Sustainable Chemistry & Engineering

Research Article

pubs.acs.org/journal/ascecg

Sulfate-Anchored Hierarchical Meso−Macroporous N-doped TiO_2: A Novel Photocatalyst for Visible Light H_2 Evolution

Soumyashree Pany[†,‡] and K. M. Parida*[,†,‡]

[†]Academy of Scientific and Innovative Research, Anusandhan Bhawan, 2 Rafi Marg, New Delhi 110 001, India

[‡]Colloids and Materials Chemistry Department, CSIR-Institute of Minerals and Materials Technology, Bhubaneswar 751 013, Odisha, India

Supporting Information

ABSTRACT: Visible light-active hierarchical meso−macroporous S,N-modified TiO_2 has been synthesized through a precipitation and deposition method and characterized by X-ray diffraction, field emission scanning electron microscopy, Fourier transform infrared spectroscopy, BET surface area, X-ray photo electron spectroscopy, and photoluminescence studies. The finding demonstrates that N exists in the form of N−Ti−O in the crystal lattice of TiO_2; however, sulfate (S^{6+}) is bidentately coordinated on the surface of TiO_2. The existence of sulfate maintains the morphology as well as enhances the surface area, decreases the crystallite size, shifts the optical absorption toward the red end, acts as co-catalyst, and facilitates the photogenerated charge carriers. Moreover, the presence of a hierarchical meso−macroporous frame enhances visible light-harvesting properties as well as favors easy channelization of electrons, which effectively reduces the charge recombination. The photocatalytic activity has been evaluated through H_2 evolution. The observed enhancement in activity for 4SNTP-400 has been explained on the basis of a synergistic combination of anionic−cationic species, hierarchical meso−macroporous frames with high surface area, and high crystallization of anatase phase with small crystallite size and low PL intensity, which makes the system more potential toward visible light activity.

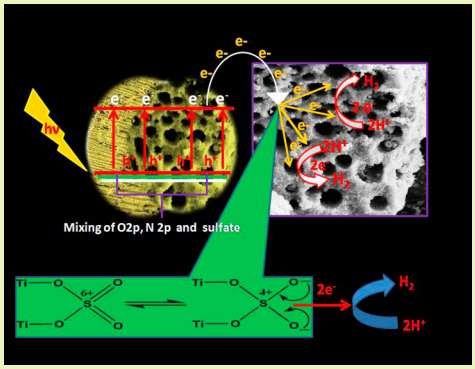

KEYWORDS: *Hierarchical, Meso−macroporous, Visible light-harvesting, Channelization, H_2 evolution*

INTRODUCTION

The development of clean energy by solar energy conversion is one of the major strategies for solving the global energy crisis and environmental problems.[1] After the important invention of Fujishima and Honda on photoelectrochemical water splitting over a TiO_2 electrode,[2] a lot of attention has been given to the development of clean, economical, and environmentally friendly production of H_2 by utilizing solar energy.[3,4]

For this solar energy conversion process as well as for environmental cleanup, a semiconductor-based visible light photocatalyst has gained broad and interdisciplinary attention for research. Among all of the oxide-based semiconductor photocatalysts, TiO_2 is considered the most appropriate candidate for photocatalytic application due to its excellent photochemical stability, cost effectiveness, and innocuousness.[5,6] However, the wide band gap, i.e, ∼3 eV, and fast recombination of electron and hole limits its application in the photocatalytic reaction process.[7] Therefore, one of the primary objectives in the field of photocatalysis is to make TiO_2 sensitive toward visible light and/or to avoid the recombination of photogenerated charge carriers. Therefore, a number of effective approaches have been widely proposed to further engineer the electronic band structure of TiO_2 such as modification with various anion and/or cation doping[8−11] or coupling with narrow band gap semiconductors.[12−14]

Among these methods, nonmetal doping (N, C, S, P, F) is considered as one potential approach to narrow the band gap of TiO_2, and it may create a midgap state that lowers the energy gap and subsequently shifts the optical absorption into the visible light region.[8,15−18] However, a tremendous success has been accomplished through N-doped TiO_2 either by mixing of nitrogen 2p state with O 2p state on the top of the valence band or creation of a N-induced mid-gap level that shifts the optical absorbance toward the visible region.[8,9] However, only through nitrogen doping the photocatalytic reactivity does not enhance very high. Moreover, it has been well reported that incorporation of sulfur has a potential role in modifing the electronic structure of TiO_2, and it appreciably enhances light absorption.[19] The synthetic condition and precursors used in the reaction process have important roles for the different oxidation states of sulfur (S^{2-}, S^{4+}, and S^{6+}) in TiO_2.[20,21] Recently, current research has focused on the combination of anions and cations or different anions together within the crystal lattice of TiO_2 such as C−S, N−C, N−F, and N−S, which dramatically enhances the photocatalytic activity.[22−25] Among the various reported co-doped systems, S,N-modified

Received: December 23, 2013
Revised: April 17, 2014
Published: April 21, 2014

TiO_2 drew a lot of interest and had better photocatalytic activities in comparison to either S or N over TiO_2.[26−28] In addition to the enhanced light-harvesting properties, bulk diffusion and surface charge transfer are the decisive factors for enhancing photocatalytic activity. To achieve the above key points, in addition to electronic modification, current researchers have developed material concerning some natural hierarchically porous morphology with high surface area.

It has been well reported that mesoporous and doped-mesoporous TiO_2 materials along with high crystalline anatase phase performed higher photocatalytic activity.[29] However, the combination of a meso−macroporous frame is desired for enhanced photocatalytic activity.[30] This is because a macroporous channel could serve as a light-transferring path for the distribution of photon energy into the inner photoactive mesoporous frame and allows light to absorb, reflect, and scatter inside the porous channel and effectively enhances the light-activated surface area within the material. In addition to the above, easy diffusion and channelization through the meso−macroporous material makes it highly efficient.[31]

Various research groups have synthesized hierarchical meso−macroporous TiO_2 by adopting different chemical synthesis procedures.[32,33] Nevertheless, without using any templating agent, hierarchical macroporous TiO_2 has been synthesized for the first time by Collins et al.[34] After that Yu et al. synthesized hierarchical meso−macroporous TiO_2 by the simple addition of tetrabutyl-titanate to pure water.[35] However, up to now, there is no report on anionic N- and cationic S-modified meso−macroporous TiO_2.

In the present study, we have synthesized S,N-modified hierarchical meso−macroporous TiO_2 by using simple a precipitation and deposition method. The photocatalytic activities of all these photocatalysts were evaluated through water splitting for the generation of H_2 energy under the irradiation of visible light. The as-prepared material has many positive aspects toward visible light photocatalysis such as small crystallite size, high crystalline anatase phase, enhanced light-harvesting, and high surface area due to meso−macroporous morphology. Besides this, a meso−macroporous frame enhances easy channelization of electrons, and surface-adsorbed sulfate species hinder the recombination of photogenerated charge carriers that makes the system unique and pivotal toward higher photocatalytic activity.

PREPARATION OF PHOTOCATALYST

S,N-modified hierarchical meso−macroporous TiO_2 has been synthesized through a precipitation and deposition technique. As reported earlier, a very simple precipitation method was adopted for the synthesis of N-modified hierarchical meso−macroporous TiO_2.[36] The precipitation reaction process takes only 15−20 min, and the precursors, i.e, titanium tetraisopropoxide (97% purity, Sigma-Aldrich) and ammonia (25 volume% Merck) were used without further purification.

In a typical synthesis route, 2 mL of titanium isopropoxide was added to 20 mL of 5% liquid ammonia. A white color precipitate was formed after the immediate contact of titanium isopropoxide with ammonia. After 20 min, the precipitate was filtered and washed with copious amount of water and left to dry on filter paper for 24 h, and then the samples were collected. For further S modification, different weight percentages of sulfate were loaded into the collected samples by an aqueous wetness impregnation method using H_2SO_4 (pH of the solution during the impregnation method lies in the range 3.5−4.4) and calcined at 400 °C for 2 h in an air atmosphere at a heating rate of 5 °C per minute.[37] These samples were labeled as *x*SNTP-*T*, where *T* denotes the calcination temperature and *x* denotes the various weight % of sulfate (For example, 2SNTP-400 and 4SNTP-400 for 2 and 4 wt % loading, respectively). As higher photocatalytic activity was observed for the 4SNTP-400, it was further calcined at different temperatures in the range of 500−700 °C to study the changes in both chemical and morphological behavior as well as catalytic activity.

EXPERIMENTAL SECTION

Characterizations. The structure and phase identification were determined by powder X-ray diffraction (XRD, Philips 1710, Mo Kα radiation with wavelength of 0.70932 A°). Diffraction patterns were recorded at 2θ, 6° to 39° with a step of 0.01° s^{-1}. N_2 adsorption−desorption isotherms were performed at liquid nitrogen temperature (77 K) on an ASAP-2020 (an automated surface area and porosity analyzer). The surface morphology was examined through a field emission scanning electron microscope (ZEISS SUPRA 55). The diffuse reflectance spectra were recorded on UV−vis spectrometer (Varian Cary 100) in the range of 200−800 nm using boric acid as the reference. The electronic states were investigated by X-ray photoelectron spectroscopy, and it was performed on a VG Microtech Multilab ESCA 3000 spectrometer with a nonmonochromatized Mg Kα X-ray source. The energy resolution of the spectrometer was set at 0.8 eV with Mg Kα radiation at a pass energy of 50 eV. The binding energies obtained in the XPS were corrected with a reference to the C 1s peak of carbon at 284.9 eV. Fourier transform infrared (FT-IR) spectra of the samples were taken on a Bruker ALPHA FT-IR spectrometer with KBr as the reference sample. The acid character of the catalysts was studied from the TPD-NH_3 CHEMBET-3000 (Quntachrome, U.S.A.) analyzer equipped with a thermal conductivity detector (TCD). About 0.1 g of powder sample was contained in a quartz "U" tube and degassed at 250 ∘C for 1 h with ultrapure nitrogen gas. After cooling the sample to room temperature, NH_3 (20% NH_3 balanced with helium) gas was passed over the sample while it was heated at a rate of 10 ∘C min^{-1}, and the profile was recorded. Photoluminescence (PL) studies were carried out with a fluorescence spectrometer (Perkin Elmer LS 55).

Photocatalytic Hydrogen Production. Catalytic activity and deactivation were studied in a batch reactor. About 0.05 g of the catalyst was suspended in 50 mL of an aqueous solution containing 10 vol % of methanol solution. The solution was stirred with a magnetic stirrer to prevent the sample from settling to the bottom. Prior to irradiation, the reaction mixture was purged with nitrogen gas for removing the dissolved gases. A 125 W medium pressure Hg visible lamp was used as the light source, and a 1 M $NaNO_2$ solution was used as the UV filter. The evolved gas was collected by a water displacement technique and analyzed on a GC-17A (Shimadzu) using a 5 Å molecular sieve column and thermal conductivity detector (TCD). A comparison of the retention time of the only peak that appeared on the chromatogram with the standard confirmed that the gas was only hydrogen.

RESULTS AND DISCUSSION

XRD Characterizations. The phase structures of all these samples were studied by powdered XRD analysis. Figure 1 illustrates the XRD patterns of NTP-400 and *x*SNTP-400 (various wt % sulfate (2S, 4S, 6S) loaded NTP) photocatalyst. The study revealed that all these patterns are identical with the standard pattern of anatase phase (JCPDS-21-1272). The high intense 101 plane along with 004, 200, 105, 211, 204, 116, 220, 215, and 224 peaks correspond to anatase TiO_2. The crystallite size of all of the as-prepared samples were calculated by using the Scherrer formula (eq 1) listed in Table 1.

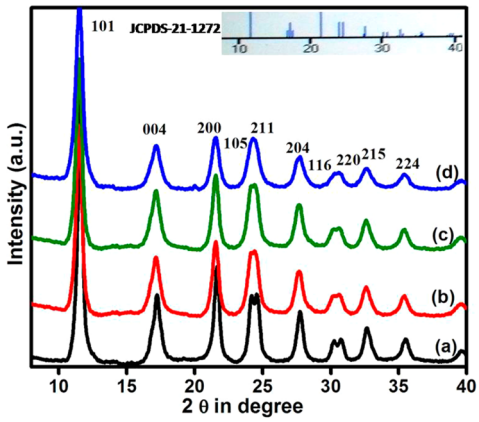

Figure 1. XRD patterns of (a) NTP-400, (b) 2SNTP-400, (c) 4SNTP-400, and (d) 6SNTP-400.

$$D = K\lambda/\beta \cos\theta \quad (1)$$

Table 1. Crystallite Size, BET Surface Area, Pore Size, Pore Volume, and Band Gap of NTP and SNTP Photocatalysts

sample code	crystallite size (nm)[a]	BET surface area (m^2/g)	pore size (Å)	pore volume (cm^3/g)	band gap (eV)
NTP-400	14.3	56	15.7	0.21	2.84
2SNTP-400	9.5	110	76.8	0.23	2.58
4SNTP-400	9.1	114	80.7	0.26	2.56
6SNTP-400	8.6	108	69.3	0.20	2.55
4SNTP-500	13.2	79.2	107	0.19	2.74
4SNTP-600	15.7	21.2	329.9	0.17	2.95
4SNTP-700	18.1	3.59	1039.0	0.09	3.0

[a]Calculated from XRD.

The XRD pattern in Figure 1 depicts that the as-prepared NTP-400 sample, along with different wt % sulfate-promoted NTP, possesses only anatase phase. The decrease in intensity of the anatase phase with an increase in broadening of the reflection in contrast to different wt % sulfate loadings suggests a gradual decrease in crystallite size. The crystallite size observed for NTP-400 is 14 nm; however, as the sulfate loading wt % increased from 2 to 6 wt %, a drastic decrease in crystallite size has been observed. The XRD patterns of 4SNTP with varying calcination temperatures from 400 to 700 °C are shown in Figure S1 of the Supporting Information. The patterns reveal that within the calcination temperature (400 to 600 °C) there is no obvious phase transformation occuring; however, at higher calcinations temperatures, i.e at 700 °C, a mixture of anatase and rutile phase has been observed. The existence of anatase phase along with small crystallite size up to 600 °C might be due to the presence of sulfate species. However, losses of sulfate species at higher calcination temperature may hinder this phenomenon, which is consistent to our earlier observation.[37,38] It has been reported that an excellent activity toward photocatalytic reaction has been found for anatase TiO_2 in contrast to rutile TiO_2.[39] As our sample 4SNTP-400 shows only anatase phase and small crystallite size, it might be one of the possible factors toward higher photocatalytic activity. In addition to this, other crucial factors toward higher photocatalytic activity are discussed later.

Surface Area. The specific surface area and interparticle mesoporosity have been studied through BET surface area by using a N_2 adsorption desorption isotherm at 77 K. The physicochemical properties of all these samples are shown in Table 1. Figure 2 represents the sorption isotherm curve, and

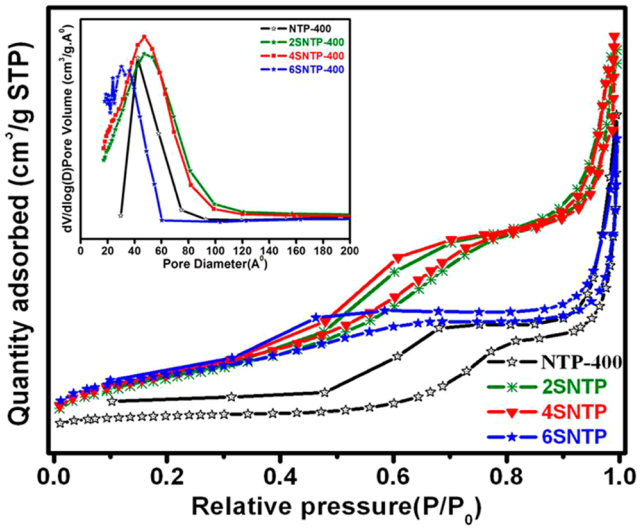

Figure 2. N_2 adsorption and desorption study of NTP-400 and *x*SNTP-400 catalysts. Inset indicates pore size distribution curves of NTP-400 and *x*SNTP photocatalysts.

the inset represents the pore size distribution curves for NTP-400 and *x*SNTP-400 (different wt % sulfate-loaded NTP) photocatalysts. The specific surface area observed for NTP-400 is 56 m^2/g; however, a drastic increase in specific surface area from 56 to114 m^2/g was observed for the sulfate-promoted NTP photocatalyst. Here, the observed-enhanced specific surface area (for *x*NTP-400) has been consistent to the crystallite size (calculated from XRD), which has a major role toward higher specific surface area.[40] All these samples exhibit type-IV isotherms, which are characteristics of mesoporous materials.[41] The hysteresis loop indicates an H_2 type, suggesting pores with wider bodies and narrow necks. The loop shape in NTP-400 clearly indicates diffusion of a bottleneck caused by pore damage, and it might be due to the extensive growth of anatase nuclei, which partly destroyed the mesoporous frame.[42] However, after sulfate loading, the anatase phase is well anchored by tetrahedral sulfate groups that hinder the crystallite growth as well as maintain the mesoporous frame. Figure S2 of the Supporting Information represents the isotherm curves for the best results performed by the 4SNTP photocatalyst with respect to different calcination temperatures. The gradual decrease in specific surface area from 114 to 20 m^2/g suggests destruction of mesoporosity, which might be due to the intergrowth of the fundamental particles. The inset in Figure 2 and Figure S2 of the Supporting Information represents the pore size distribution curves that are calculated by using the BJH equation from the desorption isotherm. From the inset in Figure 2 (for *x*SNTP-400 and NTP-400), 4SNTP-400 shows narrow and intense pore size distribution with an average pore diameter between 18.3 and 81.7 Å. This might be due to well-developed mesoporosity. However, at higher wt % sulfate loading, i.e, at 6SNTP-400, an irregular pore size distribution has been noticed in comparison to various *x*SNTP-400 photocatalysts, which might be due to excess sulfate. Sometimes an excess amount of sulfate deactivates the catalytic activity. The inset in Figure S2 of the Supporting Information

dx.doi.org/10.1021/sc400551n | ACS Sustainable Chem. Eng. 2014, 2, 1429−1438

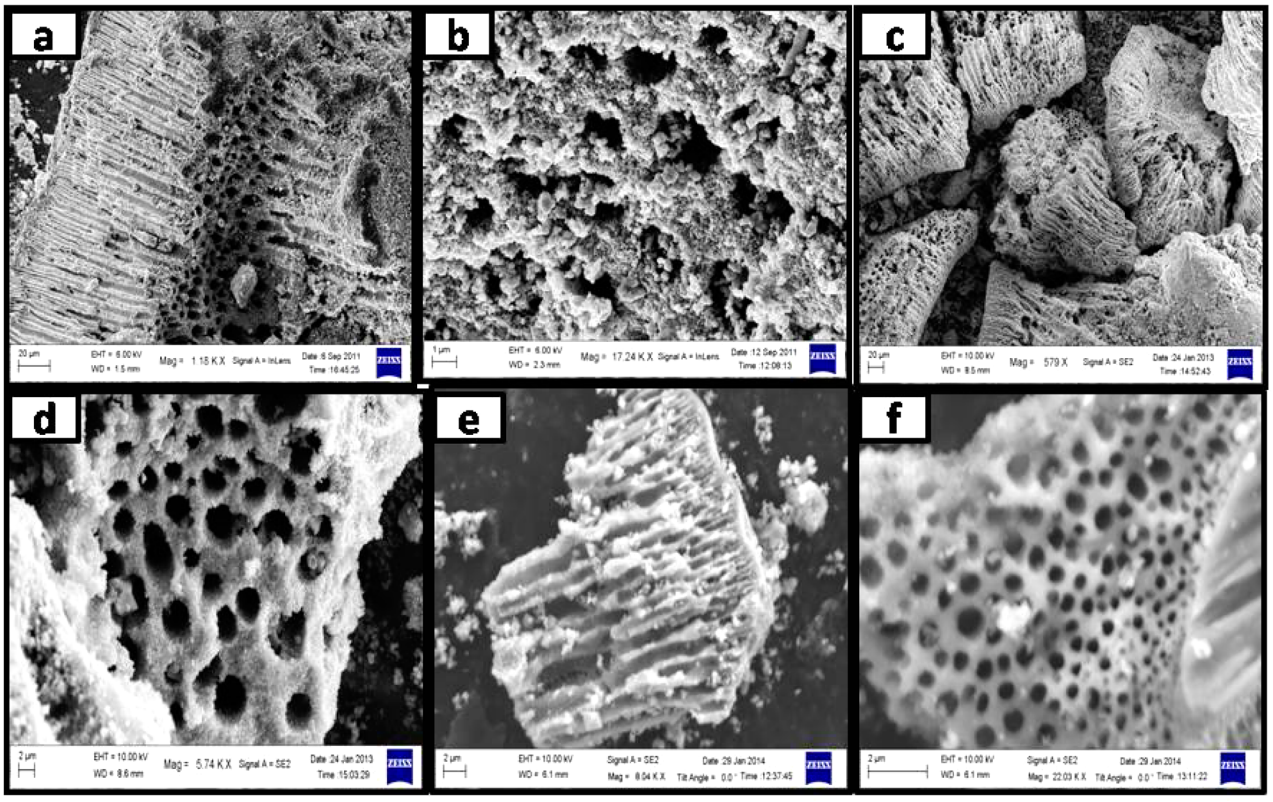

Figure 3. Micrographs for NTP-400, 4SNTP-400, and 6SNTP-400 photocatalysts.

represents the pore size distribution curve for 4SNTP with respect to variations in calcination temperatures. From the graph, a noticeable right shifting of pore size suggests an increase in pore size, which might be due to the aggregation of greater crystallite size. Among all of these, the as-prepared photocatalyst 4SNTP-400 shows higher surface area with a pore volume of 0.26 cm^3/g, which might be due to well-developed mesoporosity. For the catalytic point of view, the mesoporosity frame is potentially important because channel branching within the frame enhances the light-harvesting ability as well as decreases the diffusion length of charge carriers.

Field Emission Scanning Electron Microscopy (FESEM). The XRD analysis and N_2 sorption isotherm could not provide any information regarding macroporous morphology; therefore, field emission scanning electron microscopy (FESEM) has been performed to observe directly the macroporous frame. Figure 3 represents micrographs for NTP-400, 4SNTP-400, and 6SNTP-400 photocatalysts. Figure 3(a,b) represents micrographs for NTP-400 where (a) represents longitudinal parallel fibers with interior macroporous frames that exhibit ultralong length (60 μm) and (b) represents relatively ordered macroporous channels (2−4 μm width) arranged parallel to each other. Figure 3 (c,d) depicts micrographs for 4SNTP-400. Figure 3(c) confirms that the macroporous frame is well preserved after sulfate loading as well as maintains an ultralong length (60 μm length) and (d) depicts an ordered macroporous frame with no obvious change in its width (2−4 μm). In addition to this, the wall connecting the two macroporous frames has an equivalent width (1−2 μm) in comparison to NTP-400. Figure 3 (e,f) represents the macrographs for the 6SNTP-400 photocatalyst that reveals the formation of a hierarchical meso−macroporous frame even at higher wt % sulfate loading. The macroporous frame may act as a light-transferring and mass-transferring path that introduces photoenergy into the interior of TiO_2. The wall interconnecting the macroporous frame is composed of small interconnected TiO_2 particles having particle sizes in the range of 200−600 nm. These aggregations of smaller particles create mesoporosity and are confirmed from the N_2 sorption isotherms.

FTIR. The bonding characteristics of the functional groups have been identified by using FTIR spectroscopy. Figure 4 represents the FTIR spectrum of NTP-400 and *x*SNTP-400 photocatalysts, where as Figure S3 of the Supporting Information represents the spectrum for 4SNTP with variation in calcination temperatures, i.e., 400−700 °C. Both figures exhibit broad peaks in the region of 3000−3600 cm^{-1} assigned

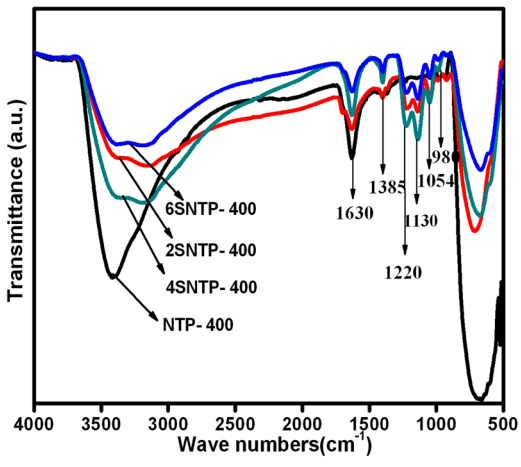

Figure 4. FTIR spectrum for NTP-400 and various wt % sulfate-loaded NTP photocatalysts.

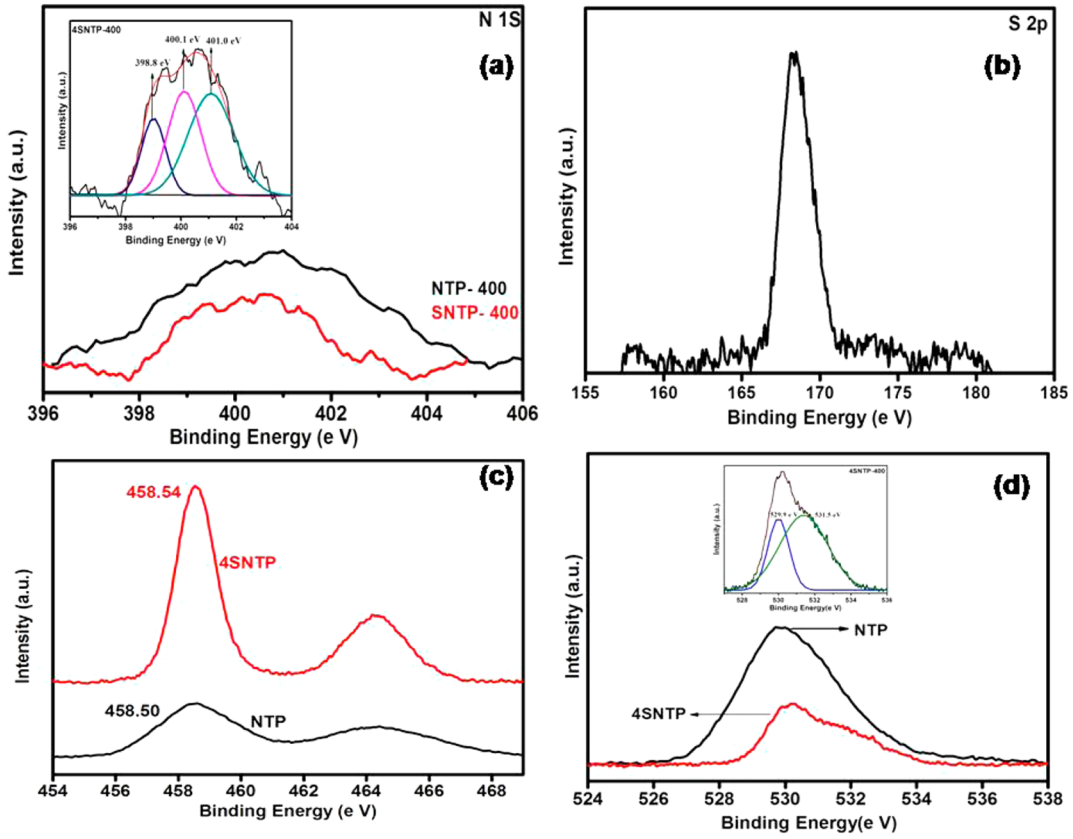

Figure 5. XPS spectra of NTP-400 and 4SNTP-400: (a) N 1s, (b) S 2p, (c) Ti 2p, and (d) O 1s.

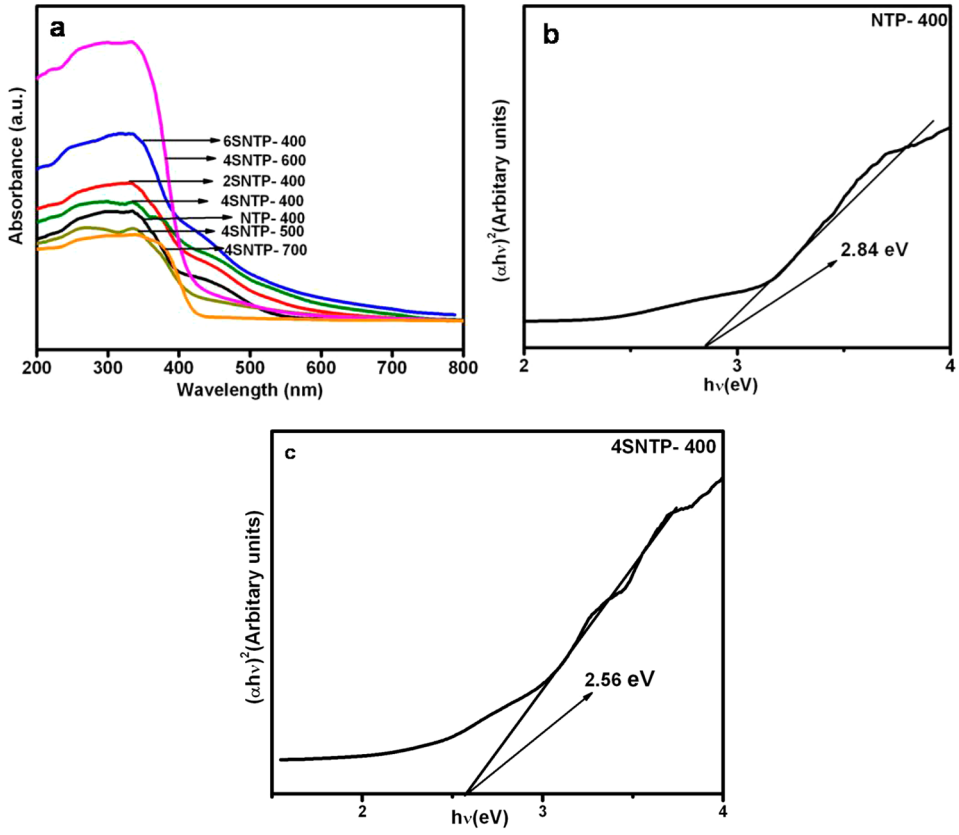

Figure 6. (a) Optical absorbance spectra of NTP-400 and *x*SNTP photocatalyst and plot of $(\alpha h\nu)^2$ vs $h\nu$ (eV) of NTP- 400 (b) and 4SNTP- 400(c).

dx.doi.org/10.1021/sc400551n | *ACS Sustainable Chem. Eng.* 2014, 2, 1429−1438

to the stretching vibration mode of adsorbed water, and another peak at 1630 cm^{-1} is attributed to the bending vibration of surface hydroxyl groups.[37] In both figures, the characteristics peak at around 1385 cm^{-1} suggests the existence of hyponitrite groups, and the peaks around 1220, 1130, 1054, and at 985 cm^{-1} are the characteristic peaks of the bidentate C_{2v} SO_4^{2-} coordinate to Ti^{4+}.[9,25,37] It has been clearly noticed from Figure S3 of the Supporting Information that sulfate species are well preserved up to 600 °C; however, at higher temperature (700 °C), no noticeable peak was found for the sulfate group, which has been consistent to the observed XRD results.

X-ray Photoelectron Spectroscopy (XPS). Figure 5 represent the XPS spectra for NTP-400 and 4SNTP-400 photocatalysts, including N 1s, S 2p, Ti 2p, and O 1s core levels.

As shown in Figure 5(a), the peak for N 1s is centered at about 400 eV. The three deconvoluted spectra for 4SNTP-400 were observed at about 398.8, 400.1, and 401.0 eV. The peak appearing at the lower energy level, i.e., at 398.8 eV, is attributed to the O−Ti−N linkage, which signifies substitution of anionic N^- in TiO_2.[36] It has been well reported that substitutional doping is more effective because it reduces the band gap by 0.13 eV and forms a localized state just above the valence band that promotes effective visible light absorption. The peaks observed at 400.1 and 401 eV might be because of a Ti−N−O environment or some surface oxidation state that also plays an important role in photocatalytic activity.[9,36] The atom percentage of N has been calculated from XPS and found to be 0.86.

Figure 5(b) depicts the S 2p core level peak appearing at about 168 eV. This peak is attributed to incorporation of SO_4^{2-} to the TiO_2 network and exists as S^{6+}.[43] As the sulfate group cannot enter into the TiO_2 lattice, it is chemisorbed into the system and forms a bidentate linkage with Ti^{4+} ions. This is also consistent with the FTIR results. The calculated atom % for S is 36.52.

Figure 5(c) reveals XPS spectrum for the Ti 2p region. For 4SNTP-400, it appeared around 458.54 eV (Ti $2p_{3/2}$) and at 463.3 eV (Ti $2p_{1/2}$), while for NTP-400, it appeared at around 458.50 eV (Ti $2p_{3/2}$). There is a difference of 0.04 eV in the binding energy value of Ti $2p_{3/2}$ between the NTP-400 and 4SNTP-400 samples. The upward shifting of 0.04 eV in the case of 4SNTP-400 might be due to the strong interaction between the bridging bidentate structures of sulfate, which withdraws electron from the Ti.[44]

Figure 5(d) depicts the O 1s spectrum. The peak appeared atabout 530 eV both for NTP-400 and 4SNTP-400. The deconvolution of the peak for 4SNTP-400 affords two peaks in the region at about 529.9 and at 531.5 eV. The peak at around 529.9 eV corresponds to oxygen in TiO_2, and the peak observed at 531.5 eV is due to the surface hydroxyl group.[45,46] From this observation, it may be concluded that nitrogen exists in two forms: one is substitutional and the other is interstitial doping. However, sulfate is bidentically coordinated to the TiO_2 matrix.

Diffuse Reflectance UV (DRUV)−Vis Spectroscopy. Figure 6 depicts the optical absorption spectra of the as-prepared SNTP and the parent NTP-400 photocatalyst. As shown in Figure 6(a), significant red shift in the absorption edge was noticed for S,N-modified TiO_2 in comparison to NTP-400. The observed band gap narrowing for the SNTP photocatalyst is directly proportional to the sulfate concentration. For a crystalline semiconductor material, the optical band gap is determined by using eq 2,[47] and the band gaps of all these samples are listed in Table 1.

$$\alpha h\nu = A(h\nu - E_g)^n \quad (2)$$

By adopting the equation, the calculated n value is 1/2, and the optical absorption is directly allowed in all these photocatalysts. As shown in Figure 6(b), the estimated direct band gap observed for NTP-400 is 2.84 eV; however, after sulfate loading, the direct band gap energies of the photocatalyst lies between 2.55 and 2.58 eV (shown in Figure 6(c) and Figure S4, Supporting Information). As shown in Figure 6(c), a noticeable absorption shift with a band gap of 2.56 eV has been noticed for 4SNTP-400. However, an increase in blue shift of the absorbance with respect to the increase in the calcination temperatures for 4SNTP (i.e., from 400 to 700 °C) has been observed in Figure S4 of the Supporting Information. The remarkable red shifting of the SNTP photocatalyst toward visible light absorbance is attributed to the coexistence of the N and S species. The N atom substitutes for O in the TiO_2 crystal, and the mixing of N 2p states with O 2p states creates a localized state just above the valence band and subsequently narrows the energy gap.[9,25,36] Furthermore, it has been well explained that in anionic and cationic S-doped TiO_2, the red shifting of the absorption band is due to the intermixing of S 3p and O 2p states.[19,48] However, a recent study reveals a narrowing of the band gap is not actually through the anion-modified TiO_2, and the observed visible light absorption results from the isolated impurity states located between the valence and conduction band.[49] It is also confirmed that substitutional N doping creates an energy state 0.14 eV above the valence band where interstitial N doping lies higher in the gap at 0.73 eV.[9,25,49] Again, the cationic S doping creates an additional S 3p level 0.38 eV above of the valence band of TiO_2.[50] The synergistic incorporation of N and S in our system creates localized states just above the valence band of TiO_2 and narrows the energy gap. The increase in blue shift of the absorbance band with respect to an increase in calcination temperatures suggests losses of S and N from the SNTP photocatalyast.[9] The red end absorption ability of SNTP has enormous importance because of further applications in direct sunlight.

NH_3 TPD. To know the acidic properties of the photocatalyst, NTP-400, 4SNTP-400, and 6SNTP-400 are subjected to NH_3 TPD analysis. The total acidity observed for NTP-400 is 0.68 mmol/g, and it is found to be lower in comparison to those of 4SNTP (2.98 mmol/g) and 6SNTP (3.9 mmol/g). From the observed result, increasing wt % of the sulfate on NTP enhances the total acidity in the catalyst, which suggests that sulfate could contribute to the total acidity of the catalyst.

Photocatalytic Activity. *Photocatalytic Hydrogen Production.* To evaluate the photocatalytic activities of all these photocatalysts (NTP-400 and xSNTP-400), photocatalytic hydrogen evolution has been carried out under visible light irradiation ($\lambda \geq 400$ nm). The reaction was performed by taking 0.05 g of catalyst in 50 mL of 10 vol % methanol solution. Before the photocatalytic reaction process, a blank experiment was carried out without the catalyst as well as with the catalyst in the absence of light. Both experiments confirmed no hydrogen evolution. The H_2 evolution for the NTP and xSNTP photocatalyst is shown in Figure 7. All these photocatalysts are active toward H_2 evolution under visible light irradiation. Among them, 4SNTP-400 shows the highest

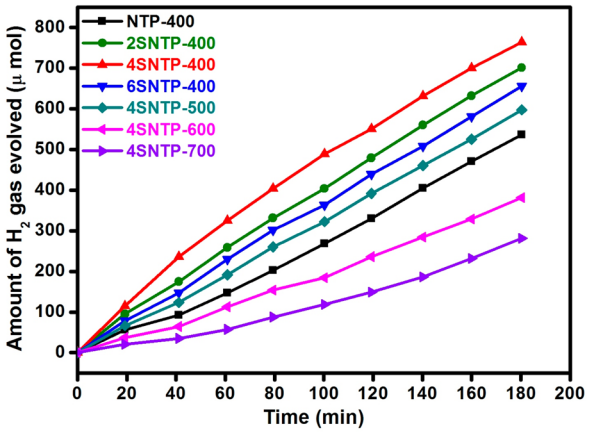

Figure 7. Time course of H_2 evolution over NTP-400 and SNTP photocatalysts.

photocatalytic activity (762.52 μmol/3h) in comparison to others as-prepared photocatalysts (*x*SNTP and NTP-400). It has been confirmed from the experiment that small amounts of sulfate incorporation (up to 4 wt %) steadily enhances the photocatalytic activity. However, further sulfate incorporation hinders the photocatalytic reaction. The recyclability test has been performed for the best result observed photocatalyst (i.e., 4SNTP-400). It has been carried out by purging N_2 gas every 3 h of the reaction and repeated for three cycles. Almost the same activity has been observed in three successive runs as shown in Figure 8.

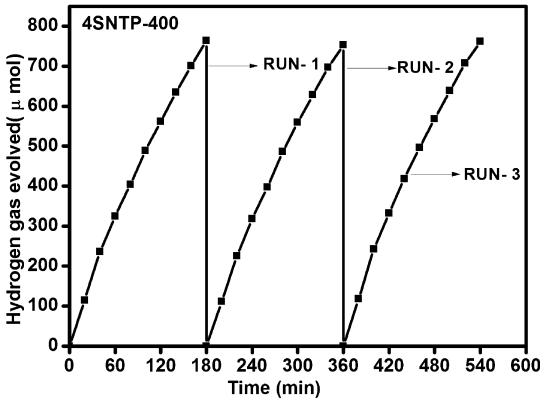

Figure 8. Reusability study over 4SNTP-400 for H_2 evolution under visible light irradiation.

In the present study, the enhanced photocatalytic activity of 4SNTP-400 can be attributed to several factors discussed as follows. It is well known that heterogeneous photocatalysis is a surface-based phenomenon; thus, larger specific surface area can provide more adsorption sites and photocatalytic reaction centers.[51] In the present case, in comparison to pure NTP-400, various wt % sulfate-loaded NTP shows enhanced specific surface area. However, a high surface area with pronounced mesoporosity (observed from pore size distribution curve) has been noticed for 4SNTP-400. It does not only introduce more reactant sites for adsorption, but also, the presence of interior macroporous channels with interconnected mesoporous frames has the basic potential role to suppress the electron−hole recombination. The presence of hierarchical macroporous morphology makes the material an artificial leaf. The morphology of an artificial leaf effectively mimics the photosynthesis of a natural leaf.[52] When the light enters through the macroporous frame, it becomes highly scattered and increases the light absorption and the optical path length. Concurrently, the light escaping from the macroporous frame is also reflected by other porous networks. The cyclic scattering and reflection enhances the light-harvesting ability.[53]In addition to the light-harvesting ability, the interconnected TiO_2 nanoparticle arrangement in the mesoporous wall may permit transportation of the highly photogenerated electron through the macroporous network. The effective light-harvesting ability as well as the inhibition of the electron−hole recombination play vital roles toward higher photocatalytic activity. As the 4SNTP-400 photocatalyst has the highest specific surface and pronounced mesoporosity, it might be the cause for the higher photocatalytic activity.

Another most crucial factor for enhanced photocatalytic activity is the incorporation of sulfate to the TiO_2 network, which extensively suppresses the anatase to rutile phase transformation as well as hinders the crystal growth during calcination. In the photocatalytic reaction process, coupling of the smaller crystallite size and high crystallinity anatase phase enhances the easy diffusion of photogenerated charge carriers toward the surface and rapidly reacts with the adsorbed reactant, which can contribute to improved photocatalytic activity. Moreover, the presence of surface acid sites may trap the photogenerated electrons. This phenomenon effectively separates the photogenerated charge carriers and prevents the recombination process, which leads to enhancing the water reduction reaction.[54] In our present study, 6SNT-400 contains 100% anatase phase and has a small crystallite size as well as the same specific surface area in comparison to 4SNTP-400, which has irregular pore size distribution and a large amount of sulfate content (i.e., 3.9 mmol/g); this might be responsible for hindering photocatalytic activity. The present result also confirms that at higher calcination temperature (500 °C), existence of sulfate species may also promote better visible light photocatalysis. However, destruction of mesoporosity due to loss of sulfate species may retard photocatalytic activity.

Considering the observed findings, a possible visible light mechanism over the 4SNTP-400 photocatalyst has been proposed and is shown in Scheme 1. Incorporation of N into the crystal lattice of TiO_2 successfully reduced the band gap by

Scheme 1. Mechanism of Photocatalytic Hydrogen Production over 4SNTP-400 Photocatalyst

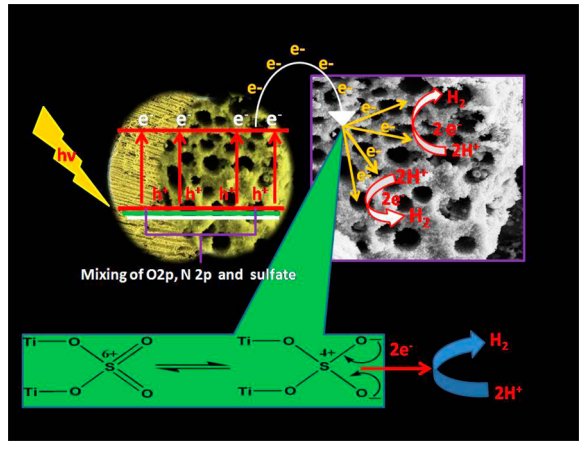

dx.doi.org/10.1021/sc400551n | ACS Sustainable Chem. Eng. 2014, 2, 1429−1438

forming a localized N 2p state just above the valence band of O 2p and helps to shift the optical absorbance toward the visible region. Incorporation of N into the crystal lattice of TiO_2 (as N−Ti−O) makes a partial conversion of Ti^{4+} to Ti^{3+} and effectively contributes to visible light absorption. Moreover, the sulfate bidentically is attached to the TiO_2 and exists as Ti−O−S. The adsorbed sulfate species enhances surface acidity and creates Bronsted and Lewis acid sites on the TiO_2 surface as well as accepts electrons and behaves as a co-catalyst.[9,25,55] The surface adsorbed co-catalyst after the light excitation acts as an antenna and collects photogenerated charge carriers from the Fermi level, which effectively enhances photocatalytic activity.[25] Here, sulfate exists as Ti−O−S in the form of S^{6+} and acts as the center to capture photo-induced electrons. The surface-adsorbed S^{6+} cation trapped photoexcited electrons from the conduction band and easily reduces the system from S^{6+} to S^{4+}.[56] The transferred electrons facilitate the water reduction process for the formation of H_2 gas on its surface. Scheme 1 illustrates the mechanism of light absorption, easy channelization and separation of photogenerated charge carriers through the meso−macroporous frame and the presence of favorable surface structures enhance the photocatalytic activity toward H_2 evolution. So overall, synergetic combination of small crystallite size, crystalline anatase phase, high specific surface area, narrow pore size distribution, meso−macroporous frame, enhanced light harvesting ability, and easy channelization of photogenerated charge carriers makes the system more potential towards visible light water-splitting.

Photoluminescence (PL). To further confirm the above mechanism, photoluminescence spectra have determined and are shown in Figure 9. The PL spectra show major peaks at around 380, 420, 440, 460, 484, and at 531 nm. The observed peak at around 380 nm is ascribed to band to band transition.[57] The peak at around 420 nm is due to self-trapped excitation delocalized on TiO_6 octahedra, whereas the peak at 440 nm is due to band edge free excitons.[9,58] The peaks at around 460, 484, and at 531 nm are due to oxygen vacancies.[9,57] In comparison to the *x*SNTP photocatalyst, a strong intense emission peak possessed by NTP-400 indicates rapid recombination of photogenerated charge carriers. However, after sulfate loading, lower intense peaks suggest less recombination of photogenerated charge carriers. The presence of sulfate ions on the surface of the TiO_2 sample favors migration of photo-induced electrons, thus improving the electron−hole separation phenomenon and exhibiting higher photocatalytic activity.

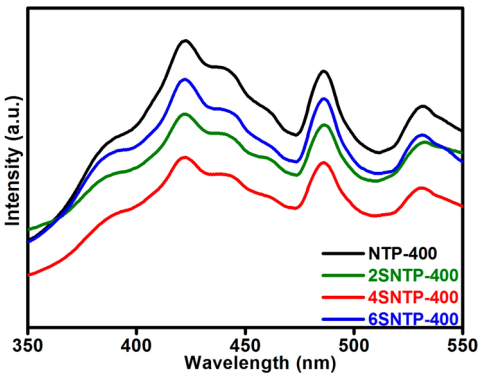

Figure 9. Photoluminescence (PL) spectra of NTP-400 and *x*SNTP-400.

CONCLUSIONS

A sulfate-anchored N-doped meso−macroporous TiO_2 photocatalyst has been fabricated by using a precipitation and deposition method. The as-prepared photocatalysts are meticulously characterized by various structural, textural, and microscopic methods. In our system, the substitutional and interstitial N incorporation as well as cationic S incorporation have played pivotal roles toward visible light absorption. Moreover, the existence of a meso−macroporous frame enhances the light-harvesting ability as well as channelizing the photogenerated charge carriers and effectively suppressing the electron−hole recombination. The excellent activity has been well supported by low PL intensity, hierarchical meso-macroporosity, smaller crystallite size, and a high crystallinity anatase phase. This study supports that S,N-modified meso−macroporous titania is a promising visible light-active photocatalyst that may have potential for effective utilization of solar light.

ASSOCIATED CONTENT

Supporting Information

XRD patterns, N_2 adsorption, and desorption studies, FTIR spectra, and plot of $(\alpha h\nu)^2$ vs $h\nu$ (eV). This material is available free of charge via the Internet at http://pubs.acs.org..

AUTHOR INFORMATION

Corresponding Author

*E-mail: paridakulamani@yahoo.com, kmparida@immt.res.in. Tel.: +91-674-2379425. Fax: +91-674-258163.

Notes

The authors declare no competing financial interest.

ACKNOWLEDGMENTS

The authors are very thankful to Prof. B. K. Mishra, Director, CSIR-IMMT, for giving permission to publish the work. The author, S. Pany, is thankful to CSIR, New Delhi, for the award of SRF. The financial assistance by CSIR in the form of NWP 56 is greatly acknowledged.

REFERENCES

(1) Maeda, K.; Domen, K. New non-oxide photocatalysts designed for overall water splitting under visible light. *J. Phys. Chem. C* **2007**, *111*, 7851−7861.

(2) Fujishima, A.; Honda, K. Electrochemical photolysis of water at a semiconductor electrode. *Nature* **1972**, *238*, 37−38.

(3) Dresselhaus, M. S.; Thomas, I. L. Alternative energy technologies. *Nature* **2001**, *414*, 332−337.

(4) Zhou, W.; Yin, Z.; Du, Y.; Huang, X.; Zeng, Z.; Fan, Z.; Liu, H.; Wang, J.; Zhang, H. Synthesis of few layer MoS_2 nanosheet-coated TiO_2 nanobelt heterostructures for enhanced photocatalytic activities. *Small* **2013**, *9*, 140−147.

(5) Hashimoto, K.; Irie, H.; Fujishima, A. TiO_2 photocatalysis: A historical overview and future prospects. *Jpn. J. Appl. Phys.* **2005**, *44*, 8269−8285.

(6) Das, P. P.; Mohapatra, S. K.; Mishra, M. Photoelectrolysis of water using heterostructural composite of TiO_2 nanotubes and nanoparticles. *J. Phys. D: Appl. Phys.* **2008**, *41*, 245103.

(7) Lin, C.; Song, Y.; Cao, L.; Chen, S. Effective photocatalysis of functional nanocomposites based on carbon and TiO_2 nanoparticles. *Nanoscale* **2013**, *5*, 4986−4992.

(8) Sivaranjani, K.; Gopinath, C. S. Porosity driven photocatalytic activity of wormhole mesoporous $TiO_{2-x}N_x$in direct sunlight. *J. Mater. Chem.* **2011**, *21*, 2639−2647.
(9) Pany, S.; Parida, K. M.; Naik, B. Facile fabrication of mesoporosity driven N−TiO_2@CS nanocomposites with enhanced visible light photocatalytic activity. *RSC Adv.* **2013**, *3*, 4976−4984.
(10) Deng, L.; Wang, S.; Liu, D.; Zhu, B.; Huang, W.; Wu, S.; Zhang, S. Synthesis, characterization of Fe-doped TiO_2 nanotubes with high photocatalytic activity. *Catal. Lett.* **2009**, *129*, 513−518.
(11) Naik, B.; Parida, K. M. Solar light active photodegradation of phenol over a $Fe_xTi_{1-x}O_{2-y}N_y$ nanophotocatalyst. *Ind. Eng. Chem. Res.* **2010**, *49*, 8339−8346.
(12) Cao, T.; Li, Y.; Wang, C.; Shao, C.; Liu, Y. A facile in situ hydrothermal method to $SrTiO_3/TiO_2$ nanofiber heterostructures with high photocatalytic activity. *Langmuir* **2011**, *27*, 2946−2952.
(13) Wu, J. M. $TiO_2/Ti_{1-x}Sn_xO_2$ heterojunction nanowires: Characterization, formation, and gas sensing performance. *J. Mater. Chem.* **2011**, *21*, 14048−14055.
(14) Yang, G.; Yan, Z.; Xiao, T. Preparation and characterization of $SnO_2/ZnO/TiO_2$ composite semiconductor with enhanced photocatalytic activity. *Appl. Surf. Sci.* **2012**, *258*, 8704−8712.
(15) Zhao, L. X.; Chen, F. X.; Wang, C.; Zhang, Y. J.; Wei, W.; Sun, Y. H.; Antonietti, M. M.; Titirici, M. One step solvothermal synthesis of a carbon@TiO_2 dyade structure effectively promoting visible-light photocatalysis. *Adv. Mater.* **2010**, *22*, 3317−3321.
(16) Samatray, S. K.; Mohapatra, P.; Parida, K. M. Physico-chemical characterization and photocatalytic activity of nanosized SO_4^{2-}/TiO_2 towards degradation of 4-nitrophenol. *J. Mol. Catal. A: Chem.* **2003**, *198*, 277−287.
(17) Samatray, S. K.; Parida, K. M. Studies on anion promoted titania-3: Effect of concentration and source of phosphate ion, method of preparation and activation temperature on redox, acid-base, textural and catalytic properties of titania. *J. Mol. Catal.* **2001**, *176*, 156−163.
(18) Wu, G.; Wang, J.; Thomas, D.; Chen, A. Synthesis of F-doped flower-like TiO_2 nanostructures with high photoelectrochemical activity. *Langmuir* **2008**, *24*, 3503−3509.
(19) Umebayashi, T.; Yamaki, T.; Itoh, H.; Asai, K. Band gap narrowing of titanium dioxide by sulfur doping. *Appl. Phys. Lett.* **2002**, *81*, 454−456.
(20) Takeshita, K.; Yamakata, A.; Ishibashi, T.; Onishi, H.; Nishijima, K.; Ohno, T. Transient IR absorption study of charge carriers photogenerated in sulfur-doped TiO_2. *J. Photochem. Photobiol., A* **2006**, *177*, 269−275.
(21) Ohno, T.; Mitsui, T.; Matsumura, M. Photocatalytic activity of S-doped TiO_2 photocatalyst under visible light. *Chem. Lett.* **2003**, *32*, 364−365.
(22) Sun, H.; Bai, Y.; Cheng, Y.; Jin, W.; Xu, N. Preparation and characterization of visible-light driven carbon-sulfur codoped TiO_2 photocatalysts. *Ind. Eng. Chem. Res.* **2006**, *45*, 4971−4976.
(23) Wang, D.; Jia, L.; Wu, X.; Lu, L.; Xu, A. One-step hydrothermal synthesis of N-doped TiO_2/C nanocomposites with high visible light photocatalytic activity. *Nanoscale* **2012**, *4*, 576−584.
(24) Li, D.; Haneda, H.; Hishita, S.; Ohashi, N. Visible-light-driven N−F co-doped TiO_2 photocatalysts. 2. Optical characterization, photocatalysis, and potential application to air purification. *Chem. Mater.* **2005**, *17*, 2596−2602.
(25) Naik, B.; Parida, K. M.; Gopinath, C. S. Facile synthesis of N^- and S^- incorporated nanocrystalline TiO_2 and direct solar light driven photocatalytic activity. *J. Phys. Chem. C* **2010**, *114*, 19473−19482.
(26) Rengifo-Herrera, J. A.; Pulgarin, C. Photocatalytic activity of N, S co-doped and N-doped commercial anatase TiO_2 powders towards phenol oxidation and *E. coli* inactivation under simulated solar light irradiation. *Sol. Energy* **2010**, *84*, 37−43.
(27) Xu, J. H.; Li, J.; Dai, W. L.; Cao, Y.; Li, H.; Fan, K. Simple fabrication of twist-like helix N,S-codoped titania photocatalyst with visible-light response. *Appl. Catal., B* **2008**, *79*, 72−80.
(28) Rengifo-Herrera, J. A.; Mielczarski, E.; Mielczarski, J. N.; Castillo, C.; Kiwi, J. *Escherichia coli* inactivation by N, S co-doped commercial TiO_2 powders under UV and visible light. *Appl. Catal., B* **2008**, *84*, 448−456.
(29) Yuan, Z. Y.; Su, B.l. Insights into hierarchically meso−macroporous structured materials. *J. Mater. Chem.* **2006**, *16*, 663−667.
(30) Wang, X.; Yu, J. C.; Ho, C.; Hou, Y.; Fu, X. Photocatalytic activity of a hierarchically macro/mesoporous titania. *Langmuir* **2005**, *21*, 2552−2559.
(31) Chen, X.; Wang, X.; Fu, X. Hierarchical macro/mesoporous TiO_2/SiO_2 and TiO_2/ZrO_2 nanocomposites for environmental photocatalysis. *Energy Environ. Sci.* **2009**, *2*, 872−877.
(32) Yu, J.; Zhang, L.; Cheng, B.; Su, Y. Hydrothermal preparation and photocatalytic activity of hierarchically sponge-like macro-/mesoporous Titania. *J. Phys. Chem. C* **2007**, *111*, 10582−10589.
(33) Xu, J.; Yang, B.; Wu, M.; Fu, Z.; Lv, Y.; Zhao, Y. Novel N−F-Codoped TiO_2 inverse opal with a hierarchical meso-/macroporous structure: synthesis, characterization, and photocatalysis. *J. Phys. Chem. C* **2010**, *114*, 15251−15259.
(34) Collins, A.; Carriazo, D.; Davis, S.; Mann, S. Spontaneous template-free assembly of ordered macroporous titania. *Chem. Commun.* **2004**, 568−569.
(35) Yu, J. G.; Su, Y.; Cheng, B. Template free fabrication and enhanced photocatalytic activity of hierarchical macro-/mesoporous titania. *Adv. Funct. Mater.* **2007**, *17*, 1984−1990.
(36) Parida, K. M.; Pany, S.; Naik, B. Green synthesis of fibrous hierarchical mesomacroporous N doped TiO_2 nanophotocatalyst with enhanced photocatalytic H_2 production. *Int. J. Hydrogen Energy* **2013**, *38*, 3545−3553.
(37) Parida, K. M.; Sahu, N.; Biswal, N. R.; Naik, B.; Pradhan, A. C. Preparation, characterization, and photocatalytic activity of sulfate-modified titania for degradation of methyl orange under visible light. *J. Colloid Interface Sci.* **2008**, *318*, 231−237.
(38) Mohapatra, P.; Moma, J.; Parida, K. M.; Jordaan, W. A.; Scurrell, M. S. Dramatic promotion of gold/titania for CO oxidation by sulfate ions. *Chem. Commun.* **2007**, 1044−1046.
(39) Martin, S. T.; Morrison, C. L.; Hoffmann, M. R. Photochemical mechanism of size-quantized vanadium-doped TiO_2 particles. *J. Phys. Chem.* **1994**, *98*, 13695−13704.
(40) Khalaf, H. A. Textural properties of sulfated iron hydroxide promoted with aluminum. *Monatsh. Chem.* **2009**, *140*, 669−674.
(41) Sing, K.; Everett, D.; Haul, R.; Moscou, L.; Pierotti, R.; Rouquerol, J.; Siemieniewska, T. Reporting physisorption data for gas/solid system with special reference to the determination of surface area and porosity. *Pure Appl. Chem.* **1985**, *57*, 603−619.
(42) Yu-de, W.; Chun-lai, M.; Xiao-dan, S.; Heng-de, L. Synthesis and characterization of mesoporous TiO_2 with wormhole-like framework structure. *Appl. Catal., A* **2003**, *246*, 161−171.
(43) Parida, K. M.; Sahu, N.; Tripathi, A. K.; Kamble, V. S. Gold promoted S,N-doped TiO_2:An efficient catalyst for CO adsorption and oxidation. *Environ. Sci. Technol.* **2010**, *44*, 4155−4160.
(44) Wang, X.; Yu, J. C.; Liu, P.; Wang, X.; Su, W.; Fu, X. Probing of photocatalytic surface sites on SO_4^{2-}/TiO_2 solid acids by in situ FTIR spectroscopy and pyridine adsorption. *J. Photochem. Photobiol., A* **2006**, *179*, 339−347.
(45) Saha, N. C.; Tompkins, H. G. Titanium nitride oxidation chemistry: An X-ray photoelectron spectroscopy study. *J. Appl. Phys.* **1992**, *72*, 3072−3079.
(46) Dong, F.; Sun, Y.; Fu, M. Enhanced visible light photocatalytic activity of V_2O_5 cluster modified N-Doped TiO_2 for degradation of toluene in air *Int. J. Photoenergy* **2012**, Article ID 569716, 1−10.
(47) Nashim, A.; Martha, S.; Parida, K. M. $Gd_2Ti_2O_7/In_2O_3$: Efficient visible-light-driven heterojunction-based composite photocatalysts for hydrogen production. *Chem. Cat. Chem.* **2013**, *5*, 2352−2359.
(48) Ohno, T. Preparation of visible light active S-doped TiO_2 photocatalysts and their photocatalytic activities. *Water Sci. Technol.* **2004**, *49*, 159−163.
(49) Etacheri, V.; Seery, M. K.; Hinder, S. J.; Pillai, S. C. Nanostructured $Ti_{1-x}S_xO_{2-y}N_y$ heterojunctions for efficient visible-light-induced photocatalysis. *Inorg. Chem.* **2012**, *51*, 7164−7173.

(50) Tian, F.; Liu, C.; Zhao, W.; Wang, X.; Wang, Z.; Yu, J. C. Cationic S-doped anatase TiO_2: A DFT study. *J. Comput. Sci. Eng.* **2011**, *1*, 33−41.
(51) Hoffmann, M. R.; Martin, S. T.; Choi, W. Y.; Bahnemann, D. W. Environmental applications of semiconductor photocatalysis. *Chem. Rev.* **1995**, *95*, 69−96.
(52) Nocera, D. G. The artificial leaf. *Acc. Chem. Res.* **2012**, *45*, 767−776.
(53) Chen, J.; Su, H.; Liu, Y.; Zeng, Y.; Zhang, W.; Gu, J.; Lau, W. M.; Zhang, D. Efficient photochemical hydrogen production under visible-light over artificial photosynthetic systems. *Int. J. Hydrogen Energy* **2013**, *38*, 8639−8647.
(54) Sasikala, R.; Shirole, A. R.; Sudarsan, V.; Kamble, V. S.; Sudakar, C.; Naik, R.; Rao, R.; Bharadwaj, S. R. Role of support on the photocatalytic activity of titanium oxide. *Appl. Catal., A* **2010**, *390*, 245−252.
(55) Pany, S.; Naik, B.; Martha, S.; Parida, K. M. Plasmon induced nano Au particle decorated over S,N-Modified TiO_2 for exceptional photocatalytic hydrogen evolution under visible light. *ACS Appl. Mater. Interfaces* **2014**, *6*, 839−846.
(56) Sun, H.; Liu, H.; Ma, J.; Wang, X.; Wang, B.; Han, L. Preparation and characterization of sulfur-doped TiO_2/Ti photoelectrodes and their photoelectrocatalytic performance. *J. Hazard. Mater.* **2008**, *156*, 552−559.
(57) Choudhury, B.; Choudhury, A. Dopant induced changes in structural and optical properties of Cr^{3+} doped TiO_2 nanoparticles. *Mater. Chem. Phys.* **2012**, *132*, 1112−1118.
(58) Mohan, R.; Drbohlavova, J.; Hubalek, J. Water-dispersible TiO_2 nano particles via a biphasic solvothermal reaction method. *Nanoscale Res. Lett.* **2013**, *8*, 503.